


Fast Spectral Characterization of Optical Passive Devices Based on Dissipative Soliton Fiber Laser Assisted Dispersive Fourier Transform

Yujia Li,[‡] Yulong Cao,^{*‡} Lei Gao, Ligang Huang, Haonan Han, Iroegbu Paul Ikechukwu[✉], and Tao Zhu[†]
*Key Laboratory of Optoelectronic Technology & Systems (Ministry of Education), Chongqing University,
 Chongqing 400044, China*

 (Received 14 February 2020; revised 22 June 2020; accepted 20 July 2020; published 25 August 2020)

Fast controllable optical passive devices containing intricate couplings of multiple physical fields, for instance, magneto-, electro-, and acousto-optic interactions, are frequently used as critical regulation tools in diverse optical systems. Their unpredictable transient spectral properties under high-speed modulation strongly influence the operational performance of the whole system, but are exhibited very little in conventional spectroscopies due to slow scans with a frame rate of the order of a kilohertz. Here, a dissipative soliton fiber laser assisted dispersive Fourier transform is built to achieve ultrafast spectroscopic characterization. An acoustically induced fiber grating (AIFG), as one typical case of a fast-response device, is studied under driving signals in frequency-switch and frequency-sweep modes. The experimental results reveal the continuous wavelength-sweeping property of the AIFG. Its transmission spectrum for a driving-frequency chirp is destroyed when the sweep time approaches the transit time of the acoustic wave in the grating region. This work opens up an avenue for the measurement of transient physical characteristics of passive devices, such as spectral aberration, transit time, and operational bandwidth.

DOI: [10.1103/PhysRevApplied.14.024074](https://doi.org/10.1103/PhysRevApplied.14.024074)

I. INTRODUCTION

Before the emergence of fast spectroscopies, the exploration of fast laser dynamics was very difficult, especially the laser generation process and the state-switching process. The coherence of the laser degenerates as a result of these processes, and the nonrepetitive transient phenomena evolve with the number of laser round trips, which makes many characterization methods invalid. If we cannot analyze these complex and unpredictable phenomena, our physical understanding of lasers is superficial, and the development of physical research on lasers and their applications will run into bottlenecks. Thanks to fast spectroscopies, a new subject named laser dynamics has attracted much attention, and is greatly broadening our understanding of lasers.

Now, a very similar situation arises with optical passive components. Controllable passive optical devices play an indispensable role in laser systems, optical sensing, and optical communications [1–3]. Obviously, the performance of such a system in an ultrahigh-speed state depends firstly on the transient response of the passive devices. Particularly, in systems with ultrafast energy-regenerative feedback, the influence of the transient properties of the device is enhanced. For example, in continuous

frequency-swept lasers, the wavelength-sweeping properties of the filters directly determine the upper limit of the sweeping speed of the lasing frequency [4]. We hope, theoretically, that the filtering peaks can be changed continuously without steps, while the filtering bandwidth remains the same when the sweep speed is increased. Moreover, if the filters cannot be in a normal working state during the tuning process, the dynamically balanced population inversion in the gain medium will be destroyed, probably resulting in the generation of huge detrimental pulses caused by strong relaxation oscillations. Therefore, the transient properties of devices need to be characterized in detail before they are used. Spectroscopy, a method frequently used for characterization of passive devices, allows measurement of many optical parameters, such as the insertion loss, Q factor, and operation band [5–8]. However, traditional spectrometers with moving scan components can analyze only static or slowly varying average spectra, and the speed reaches only the order of a kilohertz or less, which is not suitable for observing faster processes in passive devices. Other dynamic parameters, such as the response time and the wavelength-tuning speed, can be measured indirectly from intensity changes of injected signal light [9–11]. However, we are still unable to observe visualized details of the spectral evolution. If we can obtain transient spectra within a very small time interval, all transient parameters can be simultaneously obtained, which can provide more detailed guidance for the design of tunable devices and optimization of the dynamic properties of the system.

*caoyulong@cqu.edu.cn

†zhutao@cqu.edu.cn

‡These authors contributed equally to this work.

Dispersive-Fourier-transform (DFT) technology has been used in the sensing, imaging, and fast spectroscopy of active systems [12,13]. The spectrum update speed depends only on the pulse period. For example, for ultrafast lasers, a DFT can give single-shot spectra for every round trip of the pulse (of the order of a nanosecond), which allows us to observe abundant types of dynamics of ultrafast lasers, such as soliton birth, soliton explosion, optical rogue waves, and soliton molecules [14–17]. Rapid transient phenomena in these active systems can be effectively captured by the evolution of single-shot spectra. Acoustically induced fiber gratings (AIFGs) have been employed as one kind of fast passive device in tunable lasers and wavelength-division-multiplexing communications, due to their rapid tuning speed, wide tuning range, and linear tunability [18,19]. Compared with fiber Bragg gratings and long-period fiber gratings, AIFGs have much more complex dynamics, because this dynamics is generated by dynamic interactions among light fields, acoustic fields, and the fiber. Previous studies of AIFGs have focused mainly on how to improve grating structures to pursue a desired static filtering property, such as variable insertion loss, wide tuning range, no frequency shift, operational robustness, narrow bandwidth, or a steerable vector mode [20,21]. Thus, the average transmission spectrum is one of the most important experimental references, since the induced driving electrical signal is usually a standard sinusoidal signal. The wavelength-switching response time of an AIFG has been experimentally investigated in recent work, where the driving frequency was switched between two values [22]. However, the complex spectral dynamics during the switching process, such as multiple-peak spectral evolution, is still unclear. The details of this evolution also reveal the fast buildup dynamics in the AIFG at a new resonant wavelength. Besides, in many applications, the AIFG has to be driven by a frequency-swept driving signal (a sinusoidal signal with a linear frequency chirp), especially in wavelength-scanning lasers. Compared with the frequency switching, the distribution of the acoustic wave in the grating region is entirely different, where the frequency changes continuously in real time. Up to now, there has been a lack of any effective method to study theoretically or experimentally the spectral dynamics of AIFGs, including the filtering-bandwidth-maintaining property and the ability to sweep the resonant wavelength linearly during a fast tuning process. Because it is very difficult for us to drive the analytical time-varying spectrum function with the typical mode-coupling equation of an AIFG, there is no theoretical research focus on spectral evolution during the modulation of the dynamics of AIFGs.

In the experiment described in this paper, a beam from a dissipative-soliton (DS) laser is injected into a band-pass AIFG, and the output pulse is detected by a dissipative-soliton-assisted DFT (DS-DFT) system. Owing to the

flat spectrum of the DS, the spectrum obtained from the AIFG is the same as the stretched pulse profile. When the acoustic-wave driving frequency is stepped between 281 and 295 kHz, the AIFG spectrum switches periodically between two different wavelengths. The driving frequency is then set into a frequency-sweep mode with a change range of 14 kHz, and the AIFG is swept linearly over a certain wavelength range. We use the DS-DFT system to record dynamic spectra over a time interval of 124 ns, which effectively reveals various types of acousto-optical dynamics in the fiber, including the generation process in this AIFG at a new driving frequency and the bandwidth-retaining property with an enlarged frequency chirp. The experimental results also indicate that this AIFG can be employed as a linear wavelength-scanning device with a speed of over 13 000 nm/s. This paper reports a method to study the dynamics of a passive component from the perspective of fast spectral evolution, and also opens up another research dimension—the dynamics of optical passive devices.

II. PRINCIPLE AND METHOD

The principle of the measurement of the transient spectra is represented in Fig. 1. A pulsed laser with a broadband spectrum is employed as the light source for the fast measurement. Obviously, the spectral range of the light source has to match the operating wavelength band of the tested device. If the tested device operates in a static state, the spectral information is also constant, and can be easily modulated by conventional spectroscopes. However, if the spectral shape of the device varies much faster than the scanning speed of the dispersive component of the spectroscope, the conventional method is useless and provides

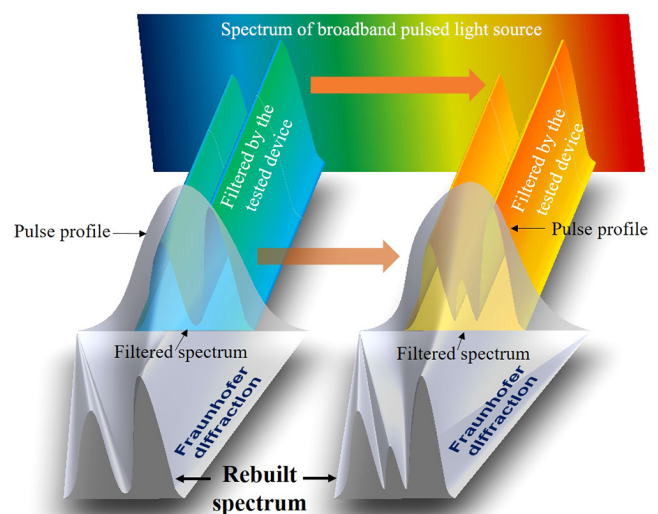


FIG. 1. Principle of the measurement of transient spectra of passive devices.

little information about the transient spectral evolution. Thus, the key point when one is measuring real-time fast-changing spectra is to improve the update frame rate. Here, the filtered spectrum successfully carries the spectral characterization of the device. Because of the strict frequency-time map, the temporal spectrum of the device can be rebuilt from the pulse profile in the time domain of the laser-source output from the tested device. Because the laser pulses are injected into the tested device in order, when the spectrum of the device changes dynamically, every pulse should carry different frequency-domain information. That is to say, the pulse period directly determines

the update speed of the spectrum obtained, which can easily reach the order of a megahertz when a soliton source is employed.

Here, we need only to consider how to achieve this rebuilding process. The DFT expands the Fraunhofer diffraction from a frequency-space map to a frequency-time map, utilizing a large-dispersion component [13]. According to the nonlinear Schrödinger equation, the evolution of the amplitude envelope of the output pulse from the tested device propagating in a dispersion component, without consideration of gain and loss, can be expressed as

$$|u(z_0, T)|^2 = \frac{1}{4\pi^2} \left| \int_{\omega_0 - \Delta\omega/2}^{\omega_0 + \Delta\omega/2} \tilde{u}_d(0, \omega - \omega_0) \tilde{u}_s(0, \omega - \omega_0) e^{j(\beta_2 z_0/2)(\omega - \omega_0 - T/\beta_2 z_0)^2} d\omega \right|^2, \quad (1)$$

where \tilde{u}_d and \tilde{u}_s represent the amplitude envelopes of the tested device and the pulse source, respectively; ω is the light frequency, ω_0 is the center frequency, β_2 is the second-order dispersion coefficient, z is the propagation distance, and T is the time in the reference frame of the pulse propagating with the group velocity, given by $T = t - \beta_1 z$. The frequency spectrum at $z = 0$ can be

driven from the time domain of the pulse profile at $z = z_0$. Compared with the tested device, the pulse source should have a much broader and flatter spectrum within the frequency range $(\omega_0 + \Delta\omega/2, \omega_0 - \Delta\omega/2)$. $|\tilde{u}_s(0, \omega - \omega_0)|^2$ is regarded as a constant, denoted by ε . If \tilde{u}_d is also a slowly varying variable with changes in ω , the equation above can be rewritten as

$$|u_d(z_0, T)|^2 \approx \frac{\varepsilon}{4\pi^2} |\tilde{u}_d(0, \omega - \omega_0)|^2 \left| \int_{\omega_0 - \Delta\omega/2}^{\omega_0 + \Delta\omega/2} e^{j(\beta_2 z_0/2)(\omega - \omega_0 - T/\beta_2 z_0)^2} d\omega \right|^2, \quad (2)$$

The integrand can contribute to the integral only when ω varies only slightly within the range $[\omega_0 + T/\beta_2 z_0 - (\pi/\beta_2 z_0)^{1/2}, \omega_0 + T/\beta_2 z_0 + (\pi/\beta_2 z_0)^{1/2}]$. Equation (2) can be rewritten further as

$$|u_d(z_0, T)|^2 \approx \frac{\varepsilon}{4\pi^2} |\tilde{u}_d(0, \omega - \omega_0)|^2 |1 + i|^2 \left(2\sqrt{\frac{\pi}{\beta_2 z_0}} \right)^2. \quad (3)$$

Because of the saddle-point approximation, $\omega \approx \omega_0 + T/\beta_2 z_0$. Therefore, the linear-map relationship between the frequency and time domains can be expressed by the equation

$$|u_d(z_0, T)|^2 \approx \frac{2\varepsilon}{\pi\beta_2 z} \left| \tilde{u}_d \left(0, \frac{T}{\beta_2 z_0} \right) \right|^2. \quad (4)$$

The term $\beta_2 z_0$ is the stretch factor of the rebuilt frequency spectrum. To ensure that the approximation in

Eq. (2) is valid, the dispersive component should have a large dispersion coefficient and ensure that the pulse has a sufficient propagation length. In the experiment described in the following, we need to select the dispersive component properly to improve the spectral resolution, according to the 3-dB spectral bandwidth of the tested component.

To characterize the dynamics of the AIFG effectively, the spectral resolution has to be smaller than the filtering bandwidth of the AIFG, and the pulse period must be much shorter than the response time of the AIFG. Because the spectrum changes continuously during the tuning process, two spectra rebuilt from two adjacent pulses may even be different from each other, as shown in Fig. 1.

In the experiment, we set the frequency-swept driving signal to have a frequency varying from f_1 to f_2 , while the time needed for this process becomes shorter and shorter [Figs. 9(a)–(d)]. Theoretically, when the sweep time of the driving frequency reaches its minimum value, the speed

of the AIFG can reach its maximum value. To explore the upper limit of the linear chirp, we can imagine an extreme situation in which the frequency f_1 is suddenly changed to f_2 , i.e., assuming that the sweep time is set to 0. However, there is also a response time for the AIFG to achieve a spectrum switch. In this case, this response time directly determines the upper limit of the wavelength-tuning speed by the equation

$$v_{\max} = R_{\text{tuning}}/\tau_{\text{res}}, \quad (5)$$

where R_{tuning} is the tuning range, and τ_{res} is the response time of the AIFG. If the sweep time is shorter than the response time, a complete frequency-sweep signal is always distributed over the grating region at any moment, and the AIFG loses its dynamic wavelength-sweeping property. Thus, the key point required to explain the measured transient dynamics that sets the upper limit of the linear chirp is to explain what determines the response time.

As shown in Fig. 2, at the moment t_1 , an acoustic wave with a frequency of f_1 just enters the grating region. At the moment t_2 , an acoustic wave with a frequency of f_2 exactly leaves the grating region, and then the transmission spectrum of the AIFG finishes the whole switching process. Thus, the response time ($\tau_{\text{res}} = t_2 - t_1$) can be calculated from the equation

$$\tau_{\text{res}} = L_{\text{ao}}/v_g, \quad (6)$$

where L_{ao} is the length of the grating region, and v_g is the group velocity of the acoustic wave. According to the equation for calculation of the group velocity, Eq. (6) can be rewritten as

$$\tau_{\text{res}} = \frac{L_{\text{ao}}}{2\sqrt{\pi RCf}}, \quad (7)$$

where R is the radius of the AIFG, C is the acoustic-wave speed in SiO_2 , and f is the driving frequency. So, the upper limits of the frequency chirp (ξ_{chirp}) and the tuning speed

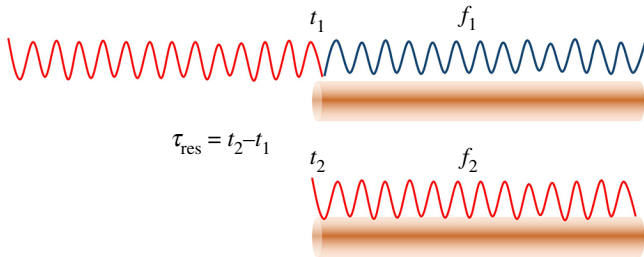


FIG. 2 Tuning-response process of an acoustically induced grating.

(v_{\max}) can be determined from the equations

$$\xi_{\text{chirp}} = \frac{f_1 - f_2}{\tau_{\text{res}}} = \frac{2(f_1 - f_2)(\sqrt{\pi RCf})}{L_{\text{ao}}}, \quad (8)$$

$$v_{\max} = \frac{R_{\text{tuning}}}{\tau_{\text{res}}} = \frac{2R_{\text{tuning}}(\sqrt{\pi RCf})}{L_{\text{ao}}}.$$

The applicability of these equations is demonstrated in the experiment described next.

III. EXPERIMENTAL SETUP

A DS having a flat rectangular spectrum with a bandwidth of 12 nm is employed as the light source for the DFT system. As shown in Fig. 3(a), the DS is generated from an all-normal-dispersion passively mode-locked fiber laser cavity. To provide a pulse of sufficient intensity for the following measurements, it is amplified by an erbium-doped fiber amplifier (EDFA) (AEDFA-23-8-FA, Amonics). The AIFG is shown in the red dashed box. An aluminum pyramid with a piezoelectric-transducer (PZT) pedestal is used to stimulate an acoustic wave from the unetched fiber cladding. The PZT is driven by a waveform generator (DG4102, Rigol) with a voltage amplifier (Model 2350, Tegam). Considering the limit of the spectral bandwidth of the DS, the whole pass-band spectral range of the AIFG should be less than 12 nm. Thus, we utilize a dispersion-compensation fiber (DCF) (DCF-G655, Changfei) with a large dispersion coefficient of 300 ps/(nm km) to compress the spectral bandwidth of the AIFG [23]. To increase the mode-coupling efficiency, the diameter of the DCF is etched to 31 μm . The band-pass AIFG is generated by acoustically induced polarization rotation, which has been studied in recent work [22]. Only the light at the resonant wavelength of the AIFG with a polarization rotation can propagate through the polarizer 2. We use polarization controller (PC) 1 to adjust the laser to provide linearly polarized light aligned with the PZT vibration direction. A refractive-index-matching fluid acting as a wave absorber can remove the acoustic-wave reflection and adjust the AIFG length.

The output laser beam from the AIFG is injected into an optical spectrum analyzer (OSA) and the DFT system for the observation of average spectra and transient spectra, respectively. The DCF (G655, YOFC) used as a pulse-stretching component in the DFT system has a length of 510 m and induces a group-delay dispersion of 200 ps/nm. The DFT technology is based on a spatiotemporal duality. Namely, the transmission of a temporal pulse in a dispersive element with a sufficiently large dispersion is analogous to the diffraction of a beam passing through a lens in the far-field approximation (Fraunhofer diffraction). The spectral information about the pulse is thus mapped into the temporal waveform of the pulse, and the stretched

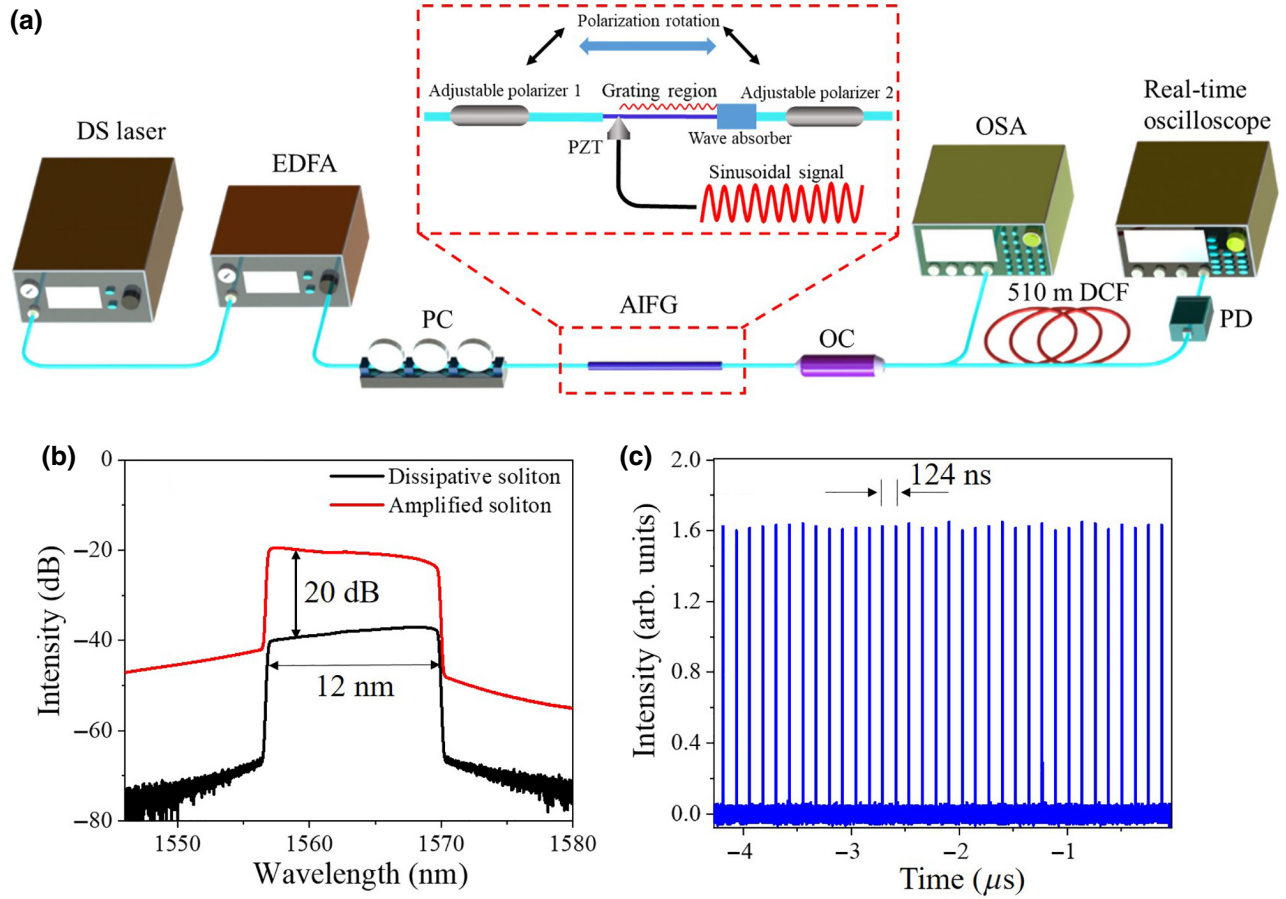


FIG. 3. (a) Experimental setup for measurement of transient spectra of the AIFG based on DS-DFT technology; (b) output average spectrum of the DS laser; (c) pulse train of the DSs. EDFA, erbium-doped fiber amplifier; PC, polarization controller; OSA, optical spectrum analyzer; DCF, dispersion-compensation fiber; PD, photodetector; OC, optical coupler.

pulse has the same shape as the spectral intensity envelope. When the above components are combined with a 50-GHz photodetector and a 20-GHz real-time oscilloscope (DSA72004B, Tektronic), the spectral resolution is 0.25 nm, calculated from the formula [13]

$$\Delta\tau = |D|L\Delta\lambda, \quad (9)$$

where $\Delta\lambda$ is the bandwidth of the spectrum, D is the group-delay dispersion per unit length of the dispersive element [usually expressed in ps/(nm km)], and $\Delta\tau$ is the minimum duration of the spectral mapping in the real-time oscilloscope. Since the 3-dB bandwidth of the AIFG is approximately 1 nm, such a resolution is sufficient to rebuild the spectral shape of the device. The black curve shown in Fig. 3(b) is a typical rectangular DS spectrum. The EDFA can amplify the DS laser by 20 dB without any spectral distortion, and the DS retains its flat spectral property, indicating a linear amplification process. The longer wavelengths of the amplified DS possess stronger energy as a result of the uneven gain of the EDFA. Figure 3(c)

shows the amplified pulse train maintaining a fundamental repetition period of 124 ns. Thus, the time interval of the transient spectrum measured by the DS-DFT system is 124 ns, which can be decreased further by utilizing a high-repetition-rate laser source.

IV. EXPERIMENTAL RESULTS AND DISCUSSION

The wavelength of the AIFG is tuned by changing the driving frequency of the acoustic wave from the waveform generator. The peak-transmission wavelength satisfies the phase-matching condition

$$\lambda = \Delta n_{\text{eff}}(\pi RC/f)^{1/2}, \quad (10)$$

where C is defined as the speed of the acoustic wave in SiO_2 , Δn_{eff} is the difference in the effective refractive index between the core mode and the cladding mode, f is the driving-signal frequency, and R is the radius of the fiber. To demonstrate that the DFT can effectively rebuild the spectral shape of the AIFG, we fix the acoustic-wave frequency, and the driving voltage is set to 1.18 V. By properly adjusting the PCs, a band-pass transmission spectrum of the

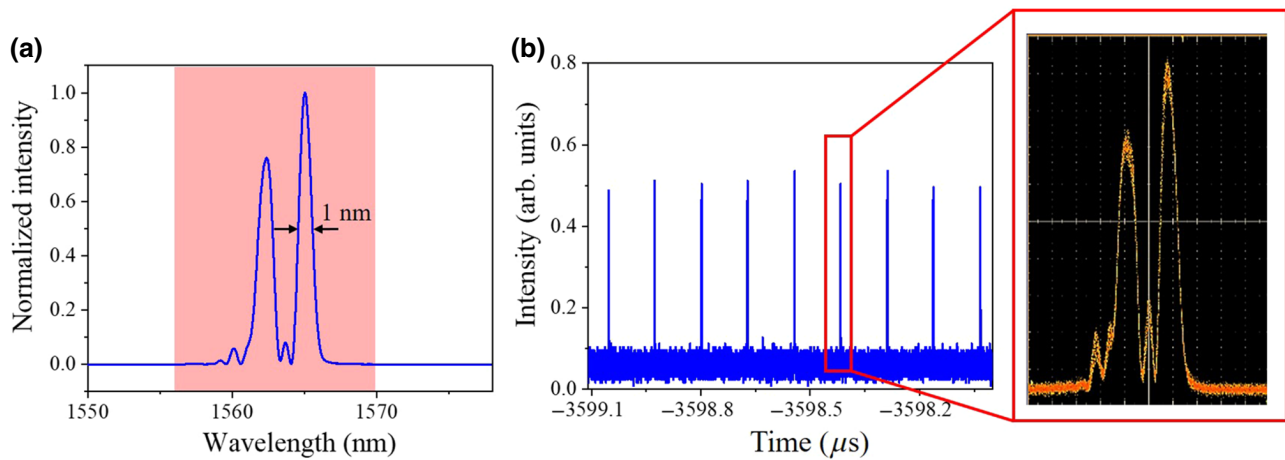


FIG. 4. (a) Average spectrum of the AIFG; the area shaded red represents the spectral range of the DS. (b) Pulse train measured by the DFT system; the inset shows the spectrum rebuilt from the pulse profile.

AIFG is achieved by use of the acoustically induced polarization rotation. Because of the vector-mode splitting in the DCF, multiple wavelengths simultaneously satisfy the resonant conditions, which generates a multiple-peak spectrum. The average transmission spectrum of the AIFG is shown in Fig. 4(a), and the spectral resolution of our OSA is 0.02 nm. The whole spectral range of the AIFG is from 1558.5 to 1566.5 nm, which is completely within the spectral range of the DS (shaded red). The 3-dB bandwidth of the right peak is 1 nm; this value is larger than the spectral resolution of our DS-DFT system. The output pulse train is shown in Fig. 4(b). The inset shows the profile of one pulse. It has the same spectral shape as the average spectrum, which coincides with Eq. (4).

Although the wavelength-switching response time of a given AIFG can be correctly estimated by use of a simple equation [22], we still want to explore the transient spectral change during this process. The driving signal is automatically switched between 281 and 295 kHz with a period of 2 ms. Figure 5(a) shows the transient spectral evolution over 4 ms (about 32 000 round trips), during which the spectrum switching completes two cycles. The intensity change between two steady states is mainly due to the uneven amplitude-frequency properties of the PZT. The dual-peak property is well retained, corresponding to the average spectrum in Fig. 4(a). To estimate the switching response time, the intensity during every round trip of the pulse is integrated with respect to time [Fig. 5(b)]. According to Eq. (7), the switching response time is approximately 280 μ s, which coincides with the transit time of the acoustic wave in the grating region, with a length of 16 cm. The buildup process of the AIFG at 295 kHz is shown in Fig. 5(c), where a complicated spectral evolution emerges during the switching process. Since the polarization states of each wavelength component of the dissipative soliton are not exactly the same [24], the

coherence of the laser after amplification is degraded, leading to an intensity jitter of about 5% after propagation through the PC. Therefore, there are subtle streaks in the demodulated real-time spectral-evolution map. Here, we emphasize the intensity evolution of the main peak at the longer wavelength, shown within the white dashed boxes. Unlike other switching mechanisms, such as those due to stress and heating, the wavelength switching includes two interesting processes. Together with the new frequency continuously covering the previous frequency, the gradual recession of the main peak at the previous resonant wavelength and the birth of a peak at the new wavelength have an overlap for a short time (in the red box). However, the spectral energy during this time is very weak. That is to say, the acousto-optical region loses almost all its grating characteristics and operates in an *off* state. Several typical spectral traces are shown in Fig. 5(d), where these two processes are indicated by the red and blue arrows. Because the extinction area within the red box is exactly located in the central region of the switching process, two waves with completely different frequencies cannot coexist in one AIFG so as to maintain a normal band-pass property.

Although the AIFG cannot achieve a continuous wavelength shift during the switching process, it can still be employed as a wavelength-scanning device by inducing frequency-swept signals. To observe its ability to achieve a continuous wavelength shift, the driving signal is set into a linear frequency-sweep mode, where the frequency changes continuously between 281 and 295 kHz. Thus, the grating region has a distribution of acoustic waves with a linear chirp frequency. Figures 6(a)–6(d) show the spectral evolution of the AIFG for sweep periods of 10, 6, 4, and 2 ms, respectively. The main peak of the AIFG spectrum has a continuous wavelength range and maintains an excellent sweep linearity, indicating that the resonant wavelength has a precise response to the driving frequency.

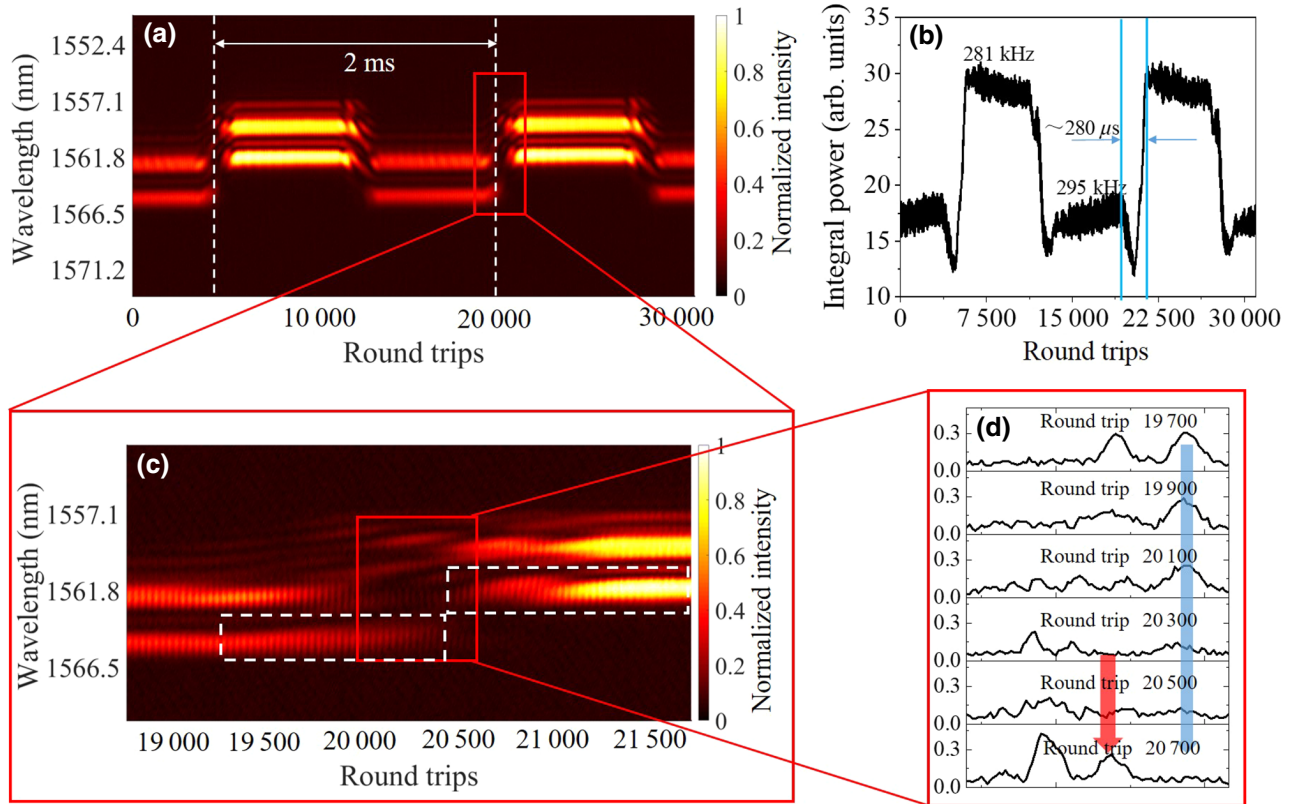


FIG. 5. (a) Two-dimensional pseudocolor map of the spectral evolution of the AIFG during 4 ms when the driving frequency is switched; (b) spectral integral power; (c) localized enlargement corresponding to the red box in Fig. 4(a); (d) several one-dimensional spectral traces from within the red box in Fig. 4(c).

When the sweep speed is increased, the multiple-peak property of the AIFG remains unchanged, coinciding with the spectra in the steady states in Fig. 6(a). The wavelength-sweeping range is equivalent to the difference in wavelength of the static spectra for driving frequencies of 281 and 295 kHz, which indicates a stable high-speed transient response. To compare the bandwidth-retaining properties of the transient spectra clearly, Fig. 7(a) shows the 3-dB bandwidth of the main peak of the transient spectrum at 1561.8 nm for different single-sweep speeds. Although the frequency chirp is increased by 5 times, the bandwidth varies only from 1.175 to 1.148 nm. The difference in value is merely 0.027 nm and is far less than the resolution of the DFT. The transmission spectra with and without a frequency chirp are also compared [Fig. 6(b)]. The black curve shows a single-shot spectrum of the AIFG driven by a sinusoidal signal with a frequency chirp of 14 kHz/ms, whereas the red curve shows a spectrum with the driving frequency fixed at 295 kHz. These two curves almost overlap, indicating that the sweep speed of the AIFG does not change the transmission spectrum even for a tuning speed of over 3000 nm. This dynamic property is very important, especially when AIFGs are used in frequency-sweep laser systems.

However, can the sweep speed within this wavelength range be increased infinitely? To observe the limitation on the sweep speed, we continue to decrease the sweep speed. In the above experimental results, the frequency increment and decrement processes occur over the same time. Here, we keep the frequency increment time (sweep time) unchanged and shorten the decrement time (return time). As shown in Fig. 8(a), the sweep time and return time are set to 1 and 0.6 ms, respectively. Both of these processes can be effectively captured by the DS-DFT system. The spectral evolution generates an asymmetric triangular wave with a period of 1.6 ms. Because of the limitation of the spectral range of the DS, the transient spectra of the AIFG are cut off at the horizontal dashed line. The other peak cannot be observed, because it is outside the spectral range of the DS. Thus, when the driving frequency is swept, the spectrum of the AIFG gradually evolves from the familiar dual-peak structure to a single-peak structure. Figures 8(b) and 8(c) plot the average spectra for driving frequencies of 297 and 281 kHz, respectively, corresponding to the trough and peak of the triangular wave in Fig. 8(a). Similarly to the previous results, the transient spectral shape coincides well with that of the average spectrum. The AIFG functions normally even for a return time

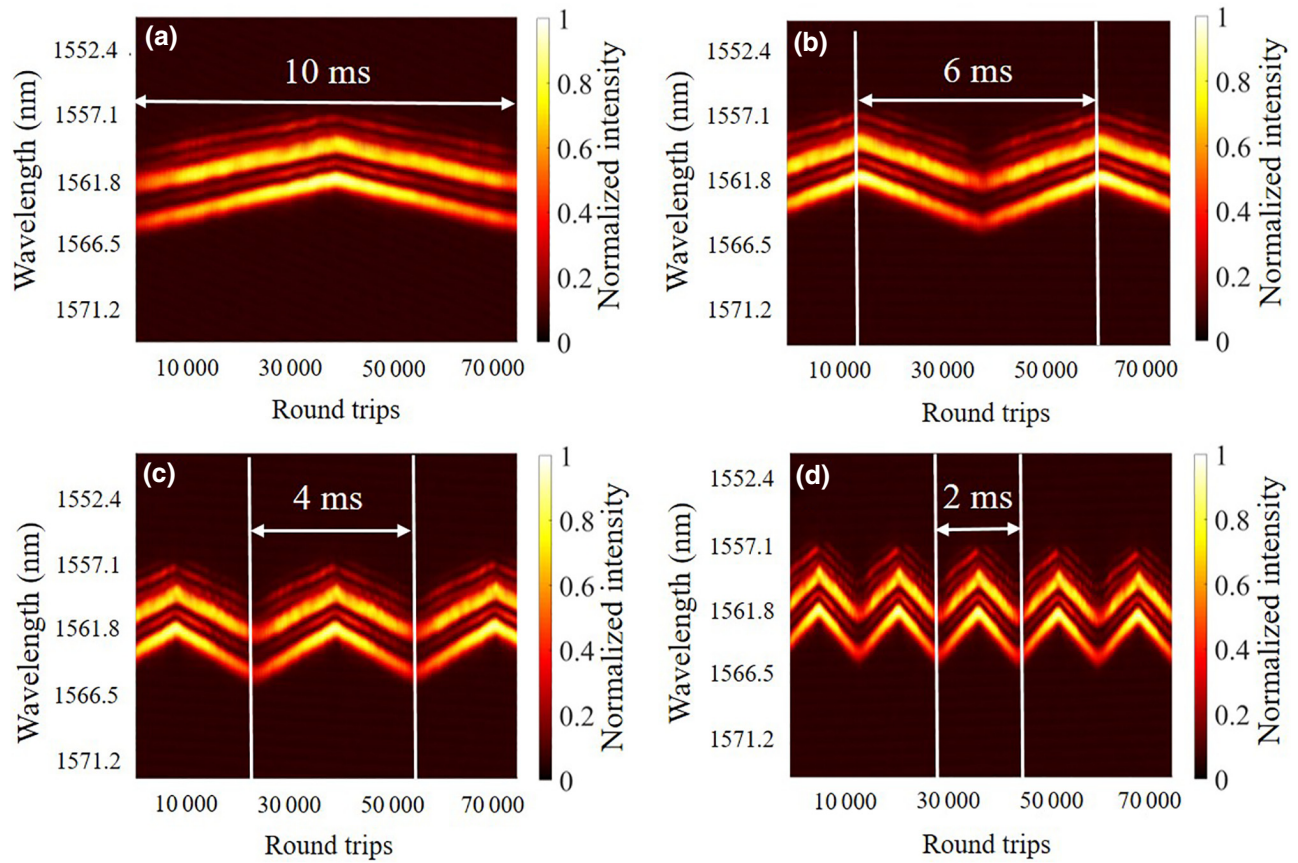


FIG. 6. (a)–(d) Two-dimensional pseudocolor maps of the spectral evolution of the AIFG for sweep periods of 10, 6, 4, and 2 ms, respectively.

of 0.6 ms. Because the DFT can rebuild only the main peak at the longer wavelength during the whole sweep range, we emphasize the spectral evolution of this peak [shown in the white box in Fig. 8(a)] in the following discussion.

To explore the upper limit on the wavelength-scanning speed within the wavelength range from 297 kHz (f_1) to 281 kHz (f_2), the return time is continuously decreased, as shown in Figs. 9(a)–9(d). The wavelength-redshift

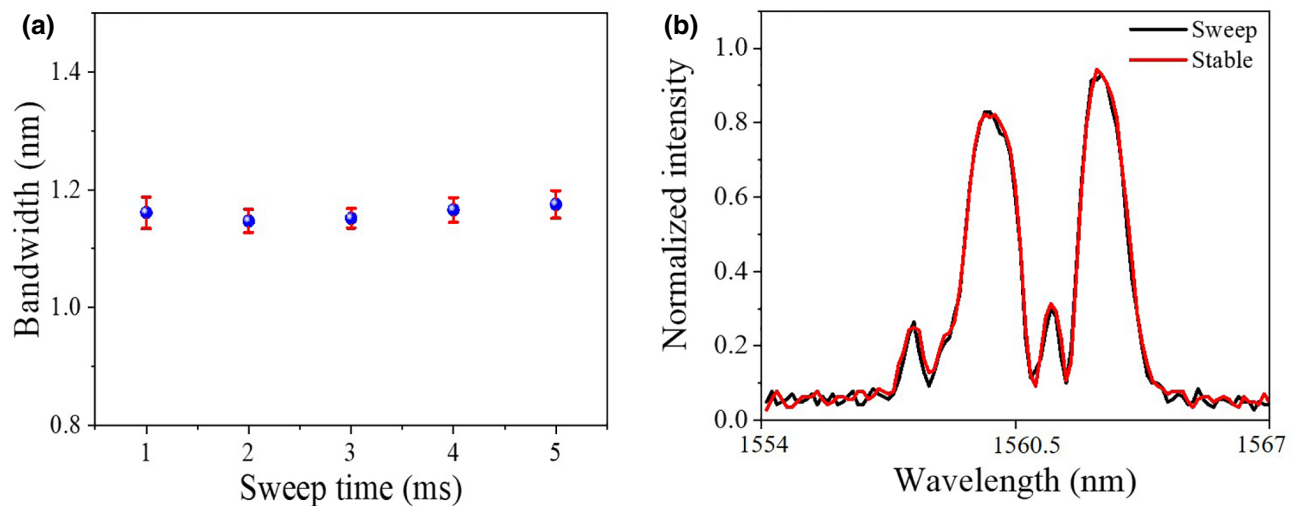


FIG. 7. (a) 3-dB bandwidth of transient spectra for sweep times of 1, 2, 3, 4, and 5 ms, for a driving frequency of 295 kHz; (b) comparison of spectra with and without a frequency chirp.

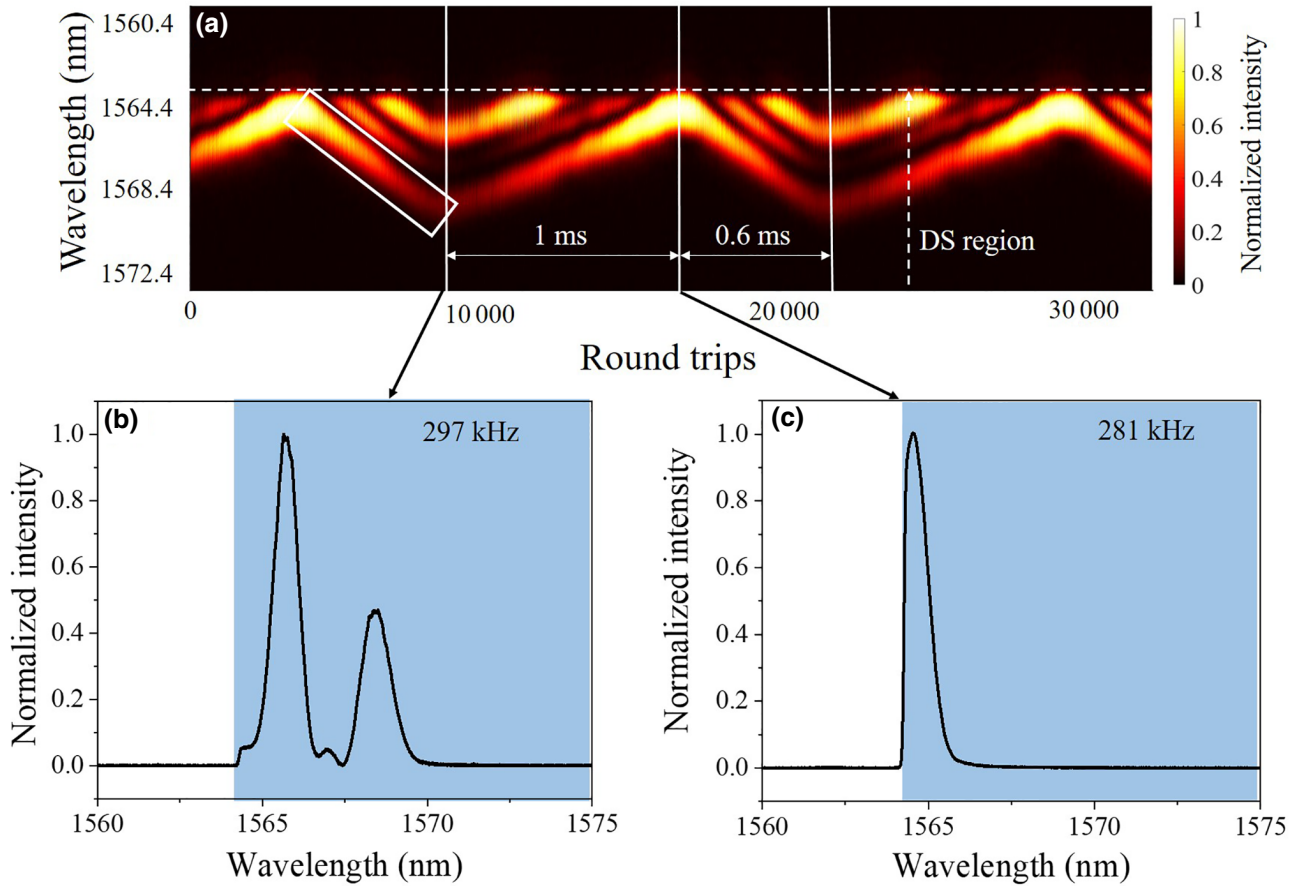


FIG. 8. (a) Two-dimensional pseudocolor maps of the spectral evolution of the AIFG for a sweep period of 1.6 ms (sweep time of 1 ms and return time of 0.6 ms); (b),(c) average spectra for driving frequencies of 297 and 281 kHz, respectively.

processes for different return times are shown in the regions between two white lines. When the return time is 0.5, 0.4, or 0.3 ms [Figs. 9(a)–(c)], the main peaks [corresponding to the peak in the white box in Fig. 8(a)] have the same wavelength-shift range of 4 nm, with an increased rate of movement. The AIFG still maintains its linear wavelength scanning for a tuning speed of over 13 000 nm/s. However, the spectral energy is suddenly interrupted when the return time is decreased to 200 μ s, as shown in the white box in Fig. 9(d). We can easily observe that the change from Fig. 9(a) to Fig. 9(c) is a gradual process, whereas the change from Fig. 9(c) to Fig. 9(d) is a mutation process. This phenomenon also coincides with what is shown in Figs. 10(a)–10(d), which show the tendency of the changes in the integral spectral power during every pulse period. The starting points of the integral power in Figs. 10(a)–10(c) are almost coincident, indicating that the original insertion loss of the AIFG is very stable. The starting point also corresponds to the endpoint of the sweep process, with an unchanged time of 1 ms. However, the following energy points decline for faster sweep speeds.

It is not difficult to understand this phenomenon of a slightly increased insertion loss [Figs. 10(a)–10(c)]. Considering a band-pass AIFG with a fixed induced driving frequency f_1 first, the mode coupling contains mainly two processes: from the core mode to the cladding mode and from the cladding mode to the core mode. Obviously, in this setup, the spectral energy that propagates through the AIFG is contributed mainly by the core-mode energy coupled from the cladding mode. When the core mode is coupled to the cladding mode for a driving frequency of f_0 , the cladding mode coupled back to the core mode should also appear at f_0 . Unfortunately, the driving frequency is always changed linearly. Therefore, the coupling process can interact only with a driving frequency of $f_0 + \xi_{\text{chirp}}t$, where ξ_{chirp} is the frequency chirp. Thus, the new resonant wavelength of the AIFG is changed, according to the phase-matching condition of the AIFG. The coupling efficiency is therefore decreased by this process. When the value of ξ is increased, the resonant wavelength interval of the two coupled processes is larger, resulting in an increased insertion loss of the AIFG. Although a large frequency chirp influences the coupling efficiency between

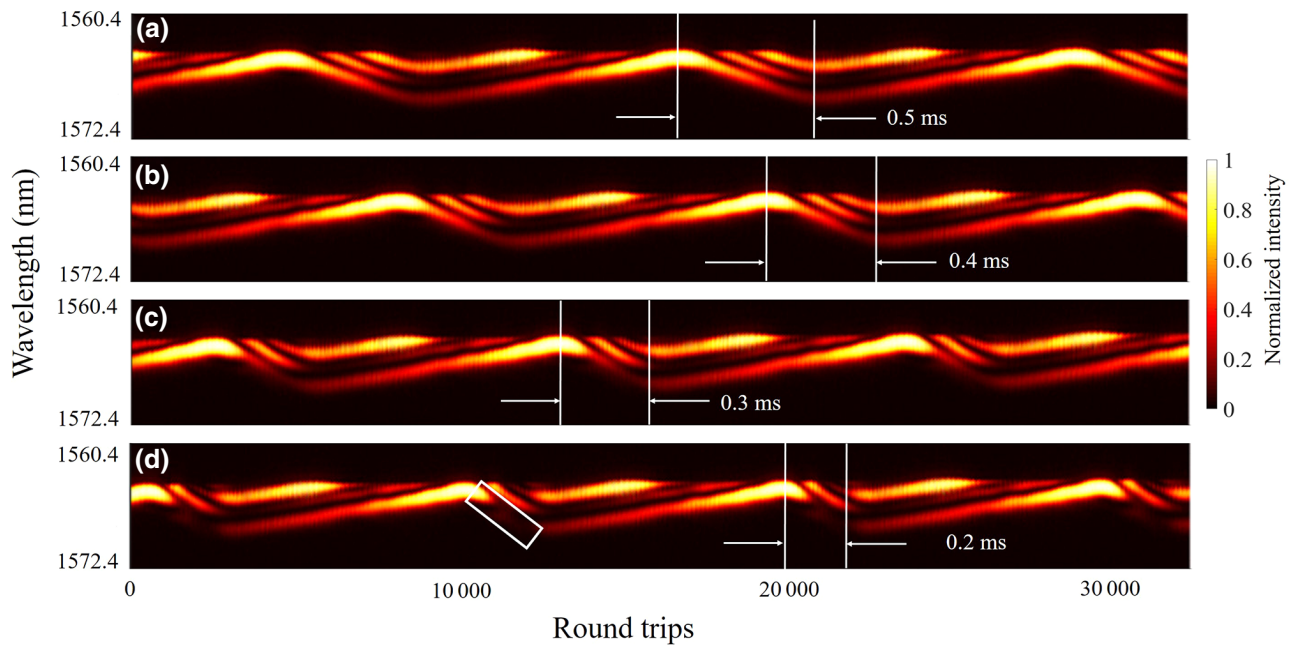


FIG. 9. (a)–(d) Two-dimensional pseudocolor maps of the spectral evolution of the AIFG for sweep periods with return times of 0.5, 0.4, 0.3, and 0.2 ms, respectively.

the cladding mode and core mode, the power evolution still has a similar trend, with just a slight energy decrement. Even for a return time of $300 \mu\text{s}$, the main peak is not interrupted during the return time, indicating a time-linear tuning property with a speed of over $13\,000 \text{ nm/s}$.

To explain the mutation phenomenon for return times between 200 and $300 \mu\text{s}$, we focus mainly on the fast return process. As the previous analysis illustrated in Fig. 5, the transit time of the acoustic wave in the AIFG is about $280 \mu\text{s}$, and this value is between these two return times.

Thus, we can consider a kind of ideal situation in which the return time exactly equals the acoustic-wave transit time in the grating region. At the beginning of the return process, a wave of frequency f_1 enters the grating region. After $280 \mu\text{s}$, this wave leaves the grating region and a wave of frequency f_2 enters the grating region, and, finally, the whole return process is ended. Thus, at the end of this process, the grating region has an acoustic-wave distribution with at most one complete sweep period. If the sweep time is continuously shortened, when the next wave of

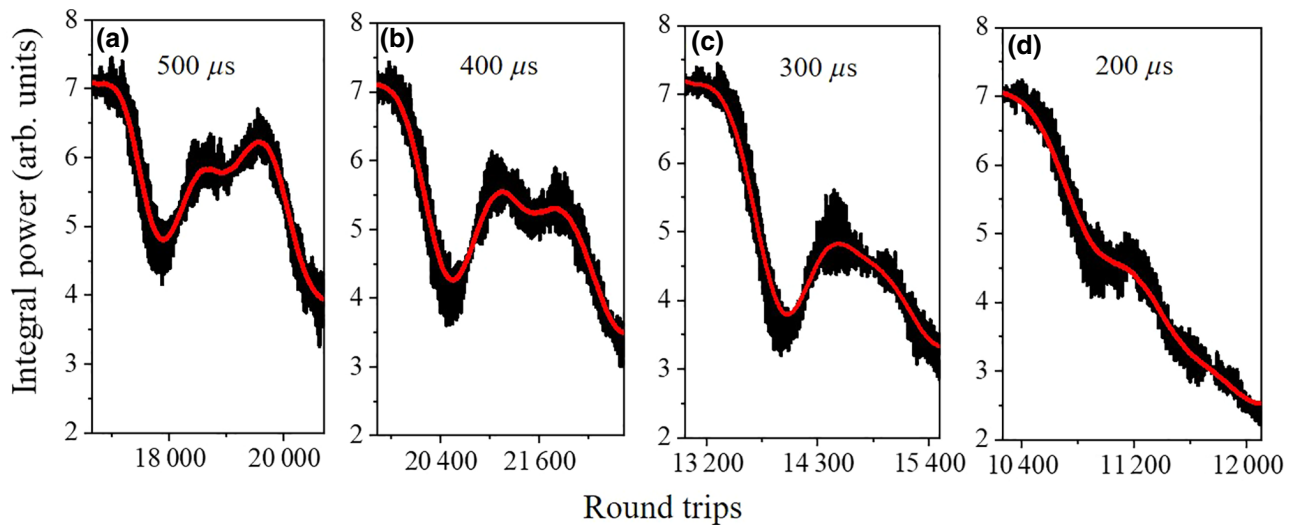


FIG. 10. (a)–(d) Tendency of change in integral power during return times of 0.5, 0.4, 0.3, and 0.2 ms, respectively.

frequency f_1 enters the grating region, the last acoustic-wave period has not yet completely left the grating region. In spite of the fact that the frequency distribution is constantly changing, the grating region always contains an acoustic wave with all frequency components from f_1 to f_2 at any time. Thus, AIFG cannot possess a preponderant resonant wavelength at one moment. Because of the abnormal acoustic-wave distribution, it is hard for the AIFG to keep a linear-sweep property, and the transmission spectra are destroyed. Therefore, if the return time is set to $300 \mu\text{s}$, this value is just slightly larger than the theoretical transit time, which is already long enough for the resonant wavelength of the AIFG to correctly respond to the changed driving frequency. The AIFG approaches closely to the limit of the frequency-sweep speed of about $13\,000 \text{ nm/s}$ within a tuning range of 4 nm , which also coincides with Eq. (8). In the experiments, we can give the spectral evolution only for return times shorten by a step size of 0.1 ms . Because of the limit on the adjustment step size of the signal generator, we cannot find a very clear time node at which we can experimentally observe the critical state of the spectral energy at the resonant wavelength. But our experiment can give an effective estimate of the maximum tuning speed of a given AIFG.

V. CONCLUSION

In the work presented in this paper, a fast spectroscopy based on the DS-DFT technology is used to investigate acousto-optical dynamics in fibers. The DS-DFT system provides single-shot spectra of an AIFG with a time interval of 124 ns , which is sufficient to distinctly observe the transient spectral evolution of the AIFG during the wavelength-switching process and the scanning process. The spectrum update frame rate can be increased further to the order of a gigahertz by utilizing higher-repetition-rate laser sources. The DS provides a rectangular spectral-shape reference, which allows the correct rebuilding of the transmission spectrum of the AIFG. We can observe that the switching process of the AIFG shows a unique wavelength mutation. The switching states have a short energy overlap, which still induces a large insertion loss before the switching process ends. The AIFG can achieve a continuous linear wavelength shift if simply a frequency-swept sinusoidal signal is induced, while the 3-dB spectrum bandwidth remains approximately 1 nm , even for a sweep time of 1 ms . The upper limit of the wavelength-sweep speed is also explored by continuously decreasing the return time. When the return time approaches the acoustic-wave transit time, it is hard for this AIFG to maintain the wavelength-scanning property, and the transmission spectrum is destroyed. Our work, employing a fast tunable AIFG as a special case, provides a method for studies of the transient dynamics of high-speed controllable passive components.

ACKNOWLEDGMENTS

This work is supported by the Natural Science Foundation of China (Grants No. 61635004, No. 61705023, and No. 61705024), the Key Research and Development Project of the Ministry of Science and Technology (Grant No. 2016YFC0801200), and the National Science Fund for Distinguished Young Scholars (Grant No. 61825501).

The authors declare that they have no competing interests.

-
- [1] N. Kobayashi, K. Sato, M. Namiwaka, K. Yamamoto, S. Watanabe, T. Kita, H. Yamada, and H. Yamazaki, Silicon photonic hybrid ring-filter external cavity wavelength tunable lasers, *J. Lightwave Technol.* **33**, 1241 (2015).
 - [2] Z. Sun, A. Martinez, and F. Wang, Optical modulators with 2D layered materials, *Nat. Photonics* **10**, 227 (2016).
 - [3] X. Gan, Y. Wang, F. Zhang, C. Zhao, B. Jiang, L. Fang, D. Li, H. Wu, Z. Ren, and J. Zhao, Graphene-controlled fiber Bragg grating and enabled optical bistability, *Opt. Lett.* **41**, 603 (2016).
 - [4] C. Jun, M. Villiger, W. Y. Oh, and B. E. Bouma, All-fiber wavelength swept ring laser based on Fabry-Perot filter for optical frequency domain imaging, *Opt. Express* **22**, 25805 (2016).
 - [5] M. Pöllinger, D. O'Shea, F. Warken, and A. Rauschenbeute, Ultrahigh-Q Tunable Whispering-Gallery-Mode Microresonator, *Phys. Rev. Lett.* **103**, 053901 (2009).
 - [6] S. Sridevi, K. S. Vasu, S. Asokan, and A. K. Sood, Enhanced strain and temperature sensing by reduced graphene oxide coated etched fiber Bragg gratings, *Opt. Lett.* **41**, 2604 (2016).
 - [7] Y. D. Shah, J. Grant, D. Hao, M. Kenney, V. Pusino, and David R. S. Cumming, Ultra-narrow line Width polarization-insensitive filter using a symmetry-breaking selective plasmonic metasurface, *ACS Photonics* **5**, 663 (2018).
 - [8] C. Fu, S. Liu, Z. Bai, J. He, C. Liao, Y. Wang, Z. Li, Y. Zhang, K. Yang, B. Yu, and Y. Wang, Orbital angular momentum mode converter based on helical long period fiber grating inscribed by hydrogen-oxygen flame, *J. Lightwave Technol.* **36**, 1683 (2018).
 - [9] W. Li, B. Chen, C. Meng, W. Fang, Y. Xiao, X. Li, Z. Hu, Y. Xu, L. Tong, H. Wang, W. Liu, J. Bao, and Y. R. Shen, Ultrafast all-optical graphene modulator, *Nano Lett.* **14**, 955 (2014).
 - [10] K. Wu, Y. Wang, C. Qiu, and J. Chen, Thermo-optic all-optical devices based on two-dimensional materials, *Photonics Res.* **6**, C22 (2018).
 - [11] S. Yu, X. Wu, K. Chen, B. Chen, X. Guo, D. Dai, L. Tong, W. Liu, and Y. R. Shen, All-optical graphene modulator based on optical Kerr phase shift, *Optica* **3**, 541 (2016).
 - [12] K. Godaa, K. K. Tsia, and B. Jalali, Amplified dispersive Fourier-transform imaging for ultrafast displacement sensing and barcode reading, *Appl. Phys. Lett.* **93**, 131109 (2008).

- [13] K. Goda and B. Jalali, Dispersive Fourier transformation for fast continuous single-shot measurements, *Nat. Photonics* **7**, 102 (2013).
- [14] G. Herink, F. Kurtz, B. Jalali, D. R. Solli, and C. Ropers, Real-time spectral interferometry probes the internal dynamics of femtosecond soliton molecules, *Science* **356**, 50 (2017).
- [15] M. Liu, A. P. Luo, W. C. Xu, and Z. C. Luo, Dissipative rogue waves induced by soliton explosions in an ultrafast fiber laser, *Opt. Lett.* **41**, 3912 (2016).
- [16] A. F. J. Runge, Neil G. R. Broderick, and Miro Eekintalo, Observation of soliton explosions in a passively mode-locked fiber laser, *Optica* **2**, 36 (2015).
- [17] X. Liu, X. Yao, and Y. Cui, Real-time Observation of the Buildup of Soliton Molecules, *Phys. Rev. Lett.* **121**, 023905 (2018).
- [18] B. Y. Kim and S. H. Yun, in *Digest of the LEOS Summer Topical Meetings* (1999), p. 6512612.
- [19] K. S. Hong, H. C. Park, and B. Y. Kim, 1000 nm tunable acousto-optic filter based on photonic crystal fiber, *Appl. Phys. Lett.* **92**, 031110 (2008).
- [20] K. Wei, W. Zhang, L. Huang, D. Mao, F. Gao, T. Mei, and J. Zhao, Generation of cylindrical vector beams and optical vortex by two acoustically induced fiber gratings with orthogonal vibration directions, *Opt. Lett.* **25**, 2733 (2017).
- [21] L. Huang, W. Zhang, Y. Li, H. Han, X. Li, P. Chang, F. Gao, G. Zhang, L. Gao, and T. Zhu, Acousto-optic tunable bandpass filter based on acoustic-flexural-wave-induced fiber birefringence, *Opt. Lett.* **43**, 5431 (2018).
- [22] Y. Li, L. Huang, H. Han, L. Gao, Y. Cao, Y. Gong, W. Zhang, F. Gao, I. P. Ikechukwu, and T. Zhu, Acousto-optic tunable ultrafast laser with vector-mode-coupling-induced polarization conversion, *Photonics Res.* **7**, 798 (2019).
- [23] H. Han, Y. Li, L. Huang, L. Gao, W. Huang, M. Liu, and T. Zhu, Dual-wavelength narrowband all-fiber acousto-optic tunable bandpass filter based on dispersion-compensating fiber, *Appl. Phys. Express* **12**, 122008 (2019).
- [24] L. Gao, Y. Cao, S. Wabnitz, H. Ran, L. Kong, Y. Li, W. Huang, L. Huang, D. Feng, and T. Zhu, Polarization evolution dynamics of dissipative soliton fiber laser, *Photonics Res.* **7**, 1331 (2019).